In vivo Tracing of the Ascending Vagal Projections to the Brain with Manganese Enhanced Magnetic Resonance Imaging

Steven Oleson[1], Jiayue Cao[2], Xiaokai Wang[2], Zhongming Liu[2,3*]

[1]*Weldon School of Biomedical Engineering, Purdue University, West Lafayette, United States*

[2]*Department of Biomedical Engineering, University of Michigan, Ann Arbor, United States*

[3]*Department of Electrical Engineering Computer Science, University of Michigan, Ann Arbor, United States*

***Correspondence**

Zhongming Liu, Ph.D.

Associate Professor of Biomedical Engineering

Associate Professor of Electrical and Computer Engineering

College of Engineering, University of Michigan

Email: zmliu@umich.edu

Conflict of interest: The authors declare no competing financial interests.

Abstract

The vagus nerve is the primary neural pathway that mediates the interactions between the brain and visceral organs. However, it is incompletely understood how the vagus nerve ascends bodily signals to the brain. Here, we explored manganese-enhanced magnetic resonance imaging (MEMRI) for in vivo tracing of vagal nerve projections to the brainstem and assessing their functional dependence on cervical vagus nerve stimulation. Manganese chloride solution was injected into either the left or right nodose ganglion. T1-weighted MRI at 12 or 24 hours following the injection showed that vagal afferent neurons inside the nodose ganglion could uptake and transport manganese ions, as a surrogate of calcium ions, to the nucleus tractus solitarius in the brainstem ipsilateral to the injection side, showing about 19 to 24% contrast enhancement. Four hours of vagus nerve stimulation further promoted nerve activity and resulted in greater contrast enhancement of 40 to 43%. These results demonstrate the feasibility of using MEMRI for structural and functional assessment of vagal afferents and their influences on brain activity.

Keywords

manganese-enhanced magnetic resonance imaging, neuronal tracing, vagus nerve, vagus nerve stimulation

Introduction

The vagus nerve is one of the essential nerves that connect the body and the brain, supporting autonomic regulations of the respiratory, cardiovascular, immune, and digestive systems (Furness et al., 2020; Howland, 2014). It contains both afferent and efferent nerve fibers, with 80% of them as afferent and ascending various bodily signals to the brain (Agostoni et al., 1957; Berthoud, & Neuhuber, 2000). The ascending vagal pathway has the cell body located at the nodose ganglion (NG) and axons projecting to the nucleus tractus solitarius (NTS) in the lower brainstem, through which it exerts widespread responses in the brain (Browning & Travagli, 2011; Cao et al., 2017; Craig, 2009). Since the cervical vagus nerve branches out to innervate and sense multiple visceral organs, it remains unclear how the brain functionally integrates the information from the ascending vagal pathway under various conditions. Although with considerable unknowns, vagus nerve stimulation (VNS) has been used as a potential treatment of many body and brain disorders, such as gastroparesis, obesity, epilepsy, Alzheimer's disease, depression, and tinnitus (Ben-Menachem, 2002; Bodenlos et al., 2007; De Ridder et al., 2014; George et al., 2000; Johnson and Wilson, 2018; Peña et al., 2013; Paulon et al., 2017; Sjogren et al., 2002). The underlying mechanisms for VNS remain unclear despite active investigations, given the complication of the vagal pathway (Johnson and Wilson, 2018). It is critical to understand the ascending vagal circuitry and how VNS could affect neural activity in the brain.

One potential approach to study the vagal circuitry is manganese-enhanced magnetic resonance imaging (MEMRI). MEMRI uses the unique properties of the manganese ion (Mn^{2+}). Mn^{2+} is a paramagnetic contrast agent. It shortens the T1 relaxation time such that Mn^{2+} accumulation increases the intensity in T1-weighted MRI (Gaggelli et al., 1983; Cory et al.,

1987; Geraldes et al., 1986). Besides, Mn^{2+} has a similar biophysical shape to the calcium ion (Ca^{2+}) and can enter neurons through voltage-gated Ca^{2+} channels (Merritt et al., 1989; Narita et al., 1990; Leung et al., 2015). Once in the neurons, Mn^{2+} could transport along axons via microtubule-dependent transport, release at the synapse, and be uptaken by adjacent post-synaptic neurons to continue the transportation along the post-synaptic neuron (Sloot & Gramsbergen, 1994; Pautler et al., 1998; Takeda et al., 1998b; Pautler & Koretsky, 2002; Pautler, 2004; Silva et al., 2004). Moreover, the rates of Mn^{2+} uptake and transportation depend on neural activity. Greater neural activity yields an increased Mn^{2+} accumulation observable with MRI (Takeda et al., 1998a&b; Tjälve et al., 1996). With these unique properties of Mn^{2+}, MEMRI has been demonstrated as a successful tracing technique to map neural pathways with activity dependency (Bearer et al., 2007; Pautler & Koretsky, 2002; Van Der Linden et al., 2002). MEMRI also overcomes the limitations of traditional tract-tracing techniques, including the invasiveness requirements to sacrifice animals and slice the brain (Pautler et al., 1998; Pautler et al., 2003; Van Der Linden et al., 2002). After neural tracing with MEMRI, other follow-up tests could be done to monitor behaviors and record neural activity on the same animal. Therefore, MEMRI could be a valuable tool to characterize the ascending vagal pathway.

In this study, we implemented MEMRI in mapping the ascending vagal pathway and adapted the MEMRI tracing protocol for tracing the bilateral vagus nerve. We first tested the feasibility of tracing the ascending vagal pathway by injecting Mn^{2+} into the NG. Then, we verified its activity dependency by applying cervical VNS to modulate vagal activity. Last, we quantified the optimal imaging time window of MEMRI. Findings and methods described herein may lay the foundation for in vivo anatomical tracing and functional characterization of the ascending vagal pathway in the rat brain.

Materials and Methods

Subjects

Nineteen rats (Sprague-Dawley, male, 320-400 g) were included in this study. The experimental procedures are approved by the Purdue Animal Care and Use Committee (PACUC). All rats were kept in a controlled environment with a 12:12 h light-to-dark cycle (lights on at 6 a.m. and off at 6 p.m.). Rats were housed in pairs in one cage until surgery and in individual cages after surgery.

Experiment design

Animals were randomly divided into three groups: groups 1 (n=9) & 2 (n=5) served as the sham control and group 3 (n=5) as the stimulation group. Animals from all three groups experienced the surgical and imaging procedures as described below and shown in Figure 1. First, all animals underwent a T1-weighted brain imaging session, termed the pre-injection MRI session. Then, rats were transported to a surgical station for NG injection of the MR contrast agent (1.0 µl of 500 mM $MnCl_2$, Sigma-Aldrich Corp., St Louis, MO, USA). A cuff electrode was implanted (Microprobes for Life Science, Gaithersburg, MD, USA) to wrap around the outside of the cervical vagus nerve. Specifically, rats in groups 1 and 3 had injections into their left NG and electrode implantation along the left cervical vagus nerve; rats in group 2 got injections into the right NG and electrode implantation along the right cervical vagus nerve. After these procedures, the rats in groups 1 and 2 had the implanted electrodes removed and recovered in their cages. The rats in stimulation group 3 experienced 4 h of VNS through the cuff

electrode. After stimulation, the electrode was removed, and the animals were allowed to recover. At 12 and 24 h after the injection, rats in all three groups were imaged again with the same T1-weighted brain MRI protocol, termed the 12 h post-injection MRI session and 24 h post-injection MRI session, respectively.

Anesthesia, MRI, and surgical protocol

Before each imaging session, animals were initially anesthetized with 5% isoflurane (oxygen, 500 mL/min) for 5 minutes. Anesthetization was maintained with 1-3% isoflurane (oxygen, 500 mL/min) throughout MR scanning. The dosage of isoflurane was adjusted depending on the monitored physiological vitals (model1030, SA instruments, Stony Brook, NY, USA). Specifically, respiratory rate and temperature were held at 40-60 cycles per minute and 37-37.5°C, respectively. For MRI, the rats were placed in a prone position in a customized rat holder. The head motion was minimized through the proper placement of a bite bar and ear bars.

The rats were scanned in a 7T horizontal-bore small animal MRI system (BioSpec 70/30; Bruker Instruments, Billerica, USA) with a gradient insert (maximum gradient: 200 mT m^{-1}; maximum slew rate: 640 $mT^{-1}s^{-1}$). A volume 1H RF coil (86 mm inner diameter) was used as the transmit coil; a ^{1}H receive-only surface coil was placed on the head as the receiver coil. To start the imaging session, we acquired a one-slice localizer and a multi-slice localizer to find the region of interest. Next, a 2D T2 Turbo RARE sequence was prescribed by locating the anterior and posterior commissures from the localizer. Lastly, a 3D T1 RARE sequence was obtained. Specifically, the 2D T2 Turbo RARE sequence was used to obtain T2-weighted images covering the brainstem (TR/TE = 6637.715/32.50ms; FA = 90°; matrix size = 192 x 192; FOV = 32mm x 32mm; slice thickness = 0.438mm; slices = 64; averages = 2). The 3D T1 RARE sequence was used to obtain T1-weighted images covering the same region (TR/TE = 300/10ms; FA = 90°;

matrix size = 192 x 192 x 64; FOV = 32mm x 32mm x 28mm; four averages). The T2-weighted and T1-weighted sequences were prescribed with the same orientation and location for the purpose of image registration.

After the pre-injection imaging session, the rats were moved to a nearby sterile surgical station for surgery. After the induced anesthesia (5% isoflurane with oxygen at 500 mL/min), the rats were laid supine and injected with carprofen (10 mg/kg, IP, Zoetis, NJ, USA). Proper anesthesia was maintained with 2% isoflurane with oxygen at 500 mL/min. The depth of anesthesia was ensured with a toe pinch test before the surgery. The rats were shaved along their neck. The exposed skin was wiped with iodine and then incised along the ventral midline from the mandible to the sternum. After the incision, the underlying tissue was dissected to visualize the trachea and left or right carotid artery. The cervical vagus nerve was identified, along with the carotid artery. The tissue connecting the carotid artery and the cervical vagus nerve was bluntly dissected to isolate the vagus nerve. The NG was then identified by following the vagus nerve rostrally. Then, the MRI contrast (1.0 µl of 500 mM $MnCl_2$) was microinjected into the NG. The microinjection was completed with a Nanofil 10 µl sub-microliter injection system with a beveled 35 gauge needle (World Precision Instruments, Sarasota, FL). To help verify the successful injection, we mixed the MRI contrast with a green dye (fast green FCF, Sigma-Aldrich, St. Louis, MO, USA), which made it possible to visualize the contrast solution inside the NG (Figure 1D). After the injection was complete, the bipolar cuff electrode (MicroProbes, Gaithersburg, MD, USA) was attached to the vagus nerve. Then, the rats in groups 1 and 2 had the electrode removed and recovered from surgery. The rats in group 3 underwent VNS along the left cervical vagus nerve for 4 h with electrical pulses (inter-pulse duration (IPD) = 50ms; pulse amplitude (PA) = 1mA; pulse width (PW) = 0.5ms; frequency =

5Hz; 20 seconds on and 40 seconds off). After stimulation, the electrode was removed for rats in group 3, and rats were allowed to recover. It was important to note that even if the rats in groups 1 & 2 did not receive VNS, all rats were implanted with the electrode to ensure similar nerve manipulation.

Image processing and statistical analysis

MR images were preprocessed using FSL (Smith et al., 2004), AFNI (Cox, 1996), and custom-developed MATLAB scripts. The anatomical T2-weighted images were linearly registered to the rat brain template (Valdés-hernández et al., 2011) using FLIRT. Again using FLIRT, the T1-weighted images were first linearly registered to the T2-weighted images and then warped to the rat brain template based on the linear relationship between the T2-weighted images and template. After preprocessing, each T1-weighted slice was normalized by its average signal intensity within the same brain slice. This normalization was completed to account for the effects of gain differences between images.

Next, the intensity increase in the post-injection images was calculated and quantified relative to the pre-injection images using a custom MATLAB script (Equation 1).

$$\Delta I = \frac{I_{post} - I_{pre}}{I_{pre}} \times 100\% \qquad \text{Equation 1}$$

In this equation, I_{post} and I_{pre} represent signal intensity in the post- and pre-injection images, respectively. ΔI is the relative intensity increase between post- and pre-injection. The relative intensity increase (ΔI) was calculated for each voxel in each animal. For each group, a right-tailed paired t-test for comparing the differences between I_{post} and I_{pre} was performed for every voxel at a confidence level of 98% (alpha = 0.02). The statistically significant voxels were highlighted in the rat brain and color-coded as averaged ΔI across animals. This statistical

procedure was completed for each experimental group and each post-injection imaging session. The maximal intensity increase was also compared between groups. Particularly, the voxel with the highest mean value of ΔI across animals in each group was first identified within the region of interest. Then, ΔI of that specific voxel was extracted for all rats within one group and compared between groups using a right-tailed two-sample t-test with a confidence level of 95% (alpha = 0.05).

Results

Feasibility of using MEMRI to trace the ascending vagal pathway

To demonstrate the feasibility of using MEMRI to trace the afferent vagal projection, we imaged the brainstem of the rats pre-injection and post-injection. The T1-weighted brainstem MRI at 24 h post-injection was compared to the pre-injection baseline (Figure 2). As shown in Figure 2, intensity increases were observed within the left NG, along the left cervical vagus nerve, within the left NTS, and to a lesser degree within the right NTS. The increased intensity suggested that the injected Mn^{2+} could enter neurons in the NG and be transported along the axon and to the downstream neurons in NTS.

To further test the specificity of the $MnCl_2$ transportation, we quantified the intensity changes of the T1-weighted images post-injection in the left (group 1, n=9) and right NG (group 2, n=5) relative to its baseline, separately. As shown in Figure 3, both groups had significant intensity increases in T1-weighted images 12 h post-injection ($p<0.02$), with the highlighted regions covering the area postrema (AP) and NTS. Also, the pattern of intensity increase depended on the injection site. The group with left NG injection had a maximum intensity increase of 23.82% in left NTS, and the group with right-side injection had a maximum intensity increase of 24.72% in right NTS. It was apparent that the intensity increase in NTS was higher on the ipsilateral side of the injection than on the contralateral side. Specifically, a higher intensity increase occurred in the left NTS in the group with left NG injection, while the higher intensity increase accumulated in the right NTS in the group with right NG injection.

VNS changes T1-weighted intensity in the ascending vagal pathway

We employed VNS to test the activity dependency of MEMRI in the ascending vagal pathway. Specifically, we compared intensity increases in T1-weighted images between rats who received VNS (group 3, n=5) and did not receive VNS (group 1, n=9) after injecting $MnCl_2$ into the left NG. The result indicated that the T1-weighted intensity increase was higher in rats who received VNS (Figure 4). At 12 h post-injection, the maximal intensity increase within the left NTS was 23.82% for rats who did not receive VNS and 42.64% for rats who received VNS, respectively; at 24 h post-injection, the maximal intensity increase within the left NTS was 21.91% for rats who did not receive VNS and 39.98% for rats who received VNS, respectively. The difference between the two groups was detectable in T1-weighted images and significant at 12 h post-injection ($p=0.0172$) and 24 h post-injection ($p=0.0187$; Figure 7), suggesting that VNS-induced higher vagal activity promoted Mn^{2+} transportation along the ascending vagus nerve and accumulation in the ipsilateral side of the NTS.

The time dependency of MEMRI when tracing the ascending vagal pathway

To evaluate the time dependency of the Mn^{2+} uptake, transportation, and accumulation, we quantified the T1-weighted intensity changes at 12 h and 24 h after injecting $MnCl_2$ into the left NG. The comparison was made for all rats who received VNS (group 3, n=5) and did not receive VNS (group 1, n=9). As shown in Figures 5 & 6, the T1-weighted intensity increase was slightly higher at 12 h post-injection compared to 24 h post-injection for both conditions. For the

group without VNS, the maximal intensity increase within the left NTS was 23.82% at 12 h post-injection and 21.91% at 24 h post-injection (Figures 5 & 7). The differences in intensity increase were similar for the group with VNS. The maximal intensity increase within the left NTS was 42.64% at 12 h post-injection and 38.98% at 24 h post-injection (Figures 6 & 7). This result suggested that the Mn^{2+} might pass the first synapse within 12 h post-injection and stay in NTS within 24 h post-injection. The T1-weighted intensity in the first-order nucleus was likely to peak within 24 h after Mn^{2+} injection.

Discussion

Here, we established the protocol of using MEMRI to trace the ascending vagal pathway noninvasively. We confirmed the feasibility of this approach by showing increased T1-weighted intensity along the vagal pathway, including the NG, the ascending vagus nerve, and NTS. These highlighted regions indicated that, by injecting $MnCl_2$ into the NG, Mn^{2+} was uptaken by neurons and transported along the vagus nerve and across the synapse. Besides, we demonstrated the activity dependency of MEMRI in tracing the ascending vagal pathway. With 4 h of VNS, NTS showed higher T1-weighted intensity than the sham condition, indicating that VNS-modulated neural activity (or likely a higher vagal tone) could affect (or increase) interneural Mn^{2+} uptake, transportation, and accumulation. Moreover, we assessed the time dependency when using MEMRI to trace the ascending vagal pathway. The T1-weighted intensity was slightly higher at 12 h in NTS on the ipsilateral side of Mn^{2+} injection than at 24 h, meaning that Mn^{2+} accumulation was likely to peak within 24 h post-injection.

MEMRI as an advanced protocol in tracing the ascending vagal pathway

Using MEMRI neural tracing protocol, we demonstrated that the T1-weighted intensity increase is observable in NTS. This finding opens a new avenue to a less-invasive approach for tracing the ascending vagal pathway in the rat brain in vivo. Compared with traditional techniques, the MEMRI protocol requires the tracing agents to be injected into the NG rather than into the brain directly. This peripheral injection is less invasive and causes less trauma to animals. Brain imaging with MRI in the MEMRI protocol is also less invasive than the

traditional technique that requires brain slicing. It is feasible to perform multiple repetitive MRI sessions for a detailed characterization of the temporal profile of the Mn^{2+} uptake, transportation, and accumulation on the same animal. Also, animals could survive for a long time after the surgery and imaging, thus allowing additional follow-up studies on the same animal. Furthermore, Mn^{2+} could pass synapses, as demonstrated in the other neural pathways (Takeda et al., 1998b; Tjälve et al., 1996). This advanced synaptic transportation property of Mn^{2+} unlocks the potential to map the ascending vagal pathway even beyond the first-order nucleus. The cross-synaptic transportation of Mn^{2+} is also activity-dependent (Bearer et al., 2007) and could be detected with MRI. When administered at a low dose, Mn^{2+} is of lower toxicity relative to virus-based neural tracing and would increase the life expectancy to merit in vivo and repeated tracing. In summary, the MEMRI protocol is a less invasive neural tracing technique that could map the functionally activated brain structures in the ascending vagal pathway across at least one synapse.

Feasibility and accuracy of using Mn^{2+} to trace the ascending vagal pathway

MEMRI neural tracing protocol utilizes the unique properties of Mn^{2+} to trace neural pathways, as first demonstrated in the mouse brain (Pautler et al., 1998). The protocol includes administering $MnCl_2$ topically to the naris for tracing the olfactory pathway and injecting $MnCl_2$ into the vitreous humor of the eye for tracing the visual pathway. Mn^{2+} was uptaken by sensory neurons in the naris and vitreous humor through voltage-dependent Ca^{2+} channels and transported in the nerve through microtubules and to the downstream neurons across synapses (Bearer et al., 2007; Lin & Koretsky, 1997; Takeda et al., 1998ab; Tjälve et al., 1996). Because

Mn^{2+} could shorten T1, the Mn^{2+} accumulation in downstream brain regions showed increased intensity in T1-weighted images, thus revealing the neuronal pathways in alive mice. Previous studies have reported T1-weighted intensity enhancement in both the axon and post-synaptic nuclei of the olfactory, visual, somatosensory, and reward pathways (Allegrini & Wiessner, 2003;Pautler et al. 1998, 2002; Pautler & Koretsky, 2001; Ryu et al., 2002; Saleem et al., 2002; Van Der Linden et al., 2002; Watanabe et al., 2001), demonstrating the feasibility and specificity of using Mn^{2+} to trace different neural pathways in alive animals.

This study applies MEMRI tracing to map the ascending vagal pathway. By injecting $MnCl_2$ into the NG, the result suggests that Mn^{2+} uptake causes the increase of T1-weighted intensity in the NG and the ascending vagus nerve. The intensity increase is also detectable in AP and NTS on the ipsilateral and contralateral sides of the injection. Specifically, the T1-weighted intensity is more elevated within NTS on the ipsilateral side of the injection and shows a slight increase on the contralateral side. The intensity increase is localized in AP, all subdivisions of the ipsilateral NTS, and more of the medial subdivisions of the contralateral NTS. These highlighted regions agree with previous findings reported with the traditional tracing technique in rats (Kalia & Sullivan, 1982), cats (Kalia & Mesulam, 1980), and lambs (Martin et al., 1991). Besides, The traditional tracing result suggests that the vagal sensory receptors primarily target heavier ipsilateral NTS than the contralateral NTS. The T1-weighted intensity map in this study reports a similar pattern, in which the intensity is higher on the ipsilateral NTS. Taken together, the MEMRI neural tracing technique could accurately map the ascending vagal pathway.

The activity dependency of MEMRI in tracing the ascending vagal pathway

MEMRI could also map neural pathways in an activity-dependent manner. As mentioned earlier, Mn^{2+} enters neurons through voltage-gated Ca^{2+} channels. Thus the neural uptake and cross-synaptic transportation of Mn^{2+} depend on neural activity (Takeda et al., 1998ab; Tjälve et al., 1996). Indeed, different degrees of neural activity cause variation in Mn^{2+} accumulation, manifesting as enhanced intensity in T1-weighted MRI with different levels at certain regions where Mn^{2+} are accumulated (Lin & Koretsky, 1997). This property qualifies MEMRI tracing in functional mapping. The feasibility has been demonstrated in the olfactory pathway (Pautler & Koretsky, 2002) and vocal-control system (Van Der Linden et al., 2002), with the elevated level of the highlighted brain regions subject to changes with different stimulation. Taken together, Mn^{2+} could not only trace anatomical connections but also map circuitries functionally with activity dependency.

Our study aligns with the previous findings and proves that MEMRI could map the ascending vagal pathway functionally. In our study, we utilize VNS to modulate neural activity in the vagus nerve and NG, which further affects neurons in downstream nuclei such as NTS. According to the previous finding in MEMRI, the changes in neural activity after Mn^{2+} administration is detectable with MRI. Consistently, our result indicates that VNS could increase T1-weighted intensity in NTS, and MEMRI could be used to map the ascending vagal pathway with activity dependency.

Future directions

While injections into the NG are not new in the traditional tract tracing protocols, using MEMRI allowed us to monitor the transportation of the tracer from the periphery to the brainstem *in vivo.* By optimizing the injection concentration, future work could explore the secondary sites of enhancement after Mn^{2+} is transported to the brainstem. The NTS has three major classes of projections, including its descending projections to autonomic preganglionic neurons within the dorsal motor vagal nucleus and the nucleus ambiguous, projections to the medullary reticular formation, and its ascending projections (Saper and Stornetta, 2015). Therefore, potential sites of enhancement for future work could assess areas such as the parabrachial nucleus (PBN), the ventroposterior parvicellular nucleus of the thalamus (VPpc), and the insular cortex (IC) (Saper and Stornetta, 2015; Herbert et al., 1990). Conceptually, for tracing these second-order brain regions and optimizing the Mn^{2+} delivery, a slow-release mechanism might be useful. This could be similar to how past studies have implemented subcutaneous osmotic pumps (Vousden et al., 2018; Poole et al., 2017) in order to help deliver the required higher doses of Mn^{2+}, while also aiding in minimizing any adverse toxic side effects.

The most advantageous use of MEMRI tract-tracing is found in incorporating the activity-dependent uptake of Mn^{2+} with its tract-tracing capabilities (Aoki et al., 2002; Lin & Koretsky, 1997; Pautler, 2004; Pautler & Koretsky, 2002; Silva et al., 2004). This technique has immense potential for studying the effects of different VNS parameters on the parasympathetic functional pathways. VNS with different parameters might modulate brain areas differently, thus activating distinct functional networks. The MEMRI tracing technique could map the functional networks activated by VNS with various parameters, contributing to a deeper understanding of the therapeutic effects of VNS. Furthermore, future work is not only limited to understanding the

effects of VNS but also being able to study the effects of other parasympathetic interventions, such as potential differences in cardiovascular and gastrointestinal conditions. With further optimization of the protocol, MEMRI might improve the understanding of vagal circuitries, map the vagal network activated at various physiological conditions, and study the effects of VNS with different parameters.

In conclusion, we have demonstrated that using MEMRI to map the ascending vagal pathway is feasible, with high specificity, and activity and time dependency. Here, we report a robust, less invasive, and contrast-enhanced MRI approach to trace neuronal connections *in vivo* over time. This method could potentially shed light on studying the effects of vagal interventions on the central nervous system.

References

Agostoni, E., Chinnock, J.E., De Burgh Daly, M., Murray, J.G., 1957. FUNCTIONAL AND HISTOLOGICAL STUDIES OF THE VAGUS NERVE AND ITS BRANCHES TO THE HEART, LUNGS, AND ABDOMINAL VISCERA IN THE CAT. Jour. Physiol. 135, 182–205.

Allegrini, P.R. and Wiessner, C., 2003. Three-dimensional MRI of cerebral projections in rat brain in vivo after intracortical injection of MnCl2. *NMR in Biomedicine: An International Journal Devoted to the Development and Application of Magnetic Resonance In Vivo*, *16*(5), pp.252-256.

Aoki, I., Tanaka, C., Takegami, T., Ebisu, T., Umeda, M., Fukunaga, M., Fukuda, K., Silva, A.C., Koretsky, A.P., 2002. Dynamic Activity-Induced Manganese-Dependent Contrast Magnetic Resonance Imaging (DAIM MRI). Magn. Reson. Med. 48, 927–933. https://doi.org/10.1002/mrm.10320

Atanasijevic, T., Bouraoud, N., Mcgavern, D.B., Koretsky, A.P., 2017. NeuroImage Transcranial manganese delivery for neuronal tract tracing using MEMRI. Neuroimage 156, 146–154. https://doi.org/10.1016/j.neuroimage.2017.05.025

Bearer, E.L., Falzone, T.L., Zhang, X., Biris, O., Rasin, A. and Jacobs, R.E., 2007. Role of neuronal activity and kinesin on tract tracing by manganese-enhanced MRI (MEMRI). *Neuroimage*, *37*, pp.S37-S46.

Ben-Menachem, E., 2002. Vagus-nerve stimulation for the treatment of epilepsy. *The Lancet Neurology*, *1*(8), pp.477-482.

Berthoud, H.R. and Neuhuber, W.L., 2000. Functional and chemical anatomy of the afferent vagal system. *Autonomic Neuroscience*, *85*(1-3), pp.1-17.

Bodenlos, J.S., Kose, S., Borckardt, J.J., Nahas, Z., Shaw, D., O'Neil, P.M. and George, M.S., 2007. Vagus nerve stimulation acutely alters food craving in adults with depression. *Appetite*, *48*(2), pp.145-153.

Browning, K. N., & Travagli, R. A., 2011. Central nervous system control of gastrointestinal motility and secretion and modulation of gastrointestinal functions. Comprehensive physiology, 4(4), 1339-1368.

Cao, J., Lu, K.H., Powley, T.L. and Liu, Z., 2017. Vagal nerve stimulation triggers widespread responses and alters large-scale functional connectivity in the rat brain. *PloS one*, *12*(12), p.e0189518.

Cory, D.A., Schwartzentruber, D.J., Mock, B.H., 1987. Ingested manganese chloride as a contrast agent for magnetic resonance imaging. Magn. Reson. Imaging 5, 65–70. https://doi.org/10.1016/0730-725X(87)90485-1

Cox, R.W., 1996. AFNI: Software for analysis and visualization of functional magnetic

resonance neuroimages. Comput. Biomed. Res. 29, 162–173. https://doi.org/10.1006/cbmr.1996.0014

Craig, A. D., 2009. How do you feel--now? The anterior insula and human awareness. Nature reviews neuroscience, 10(1).

De Ridder, D., Vanneste, S., Engineer, N.D. and Kilgard, M.P., 2014. Safety and efficacy of vagus nerve stimulation paired with tones for the treatment of tinnitus: a case series. *Neuromodulation: Technology at the Neural Interface*, *17*(2), pp.170-179.

Furness, J. B., Di Natale, M., Hunne, B., Oparija-Rogenmozere, L., Ward, S. M., Sasse, K. C., & Fothergill, L. J., 2020. The identification of neuronal control pathways supplying effector tissues in the stomach. Cell and Tissue Research, 1-13.

Gaggelli, E., Gaggelli, E., Lauterbur, P.C., 1983. Paramagnetic contrast agents in nuclear magnetic resonance medical imaging. Semin. Nucl. Med. 13, 364–376. https://doi.org/10.1016/S0001-2998(83)80048-8

Geraldes, C.F.G.C., Sherry, A.D., Brown, R.D., Koenig, S.H., 1986. Magnetic Field Dependence of Solvent Proton Relaxation Rates. Magn. Reson. Med. 250, 242–250.

George, M.S., Sackeim, H.A., Rush, A.J., Marangell, L.B., Nahas, Z., Husain, M.M., Lisanby, S., Burt, T., Goldman, J. and Ballenger, J.C., 2000. Vagus nerve stimulation: a new tool for brain

research and therapy*. *Biological psychiatry*, *47*(4), pp.287-295.

Herbert, H., Moga, M.M., Saper, C.B., 1990. Connections of the Parabrachial Nucleus With the Nucleus of the Solitary Tract and the Medullary Reticular Formation in the Rat. J. Comp. Neurol. 293, 540–580.

Howland, R.H., 2014. Vagus Nerve Stimulation. Curr Behav Neurosci Rep 64–73. https://doi.org/10.1002/bjs.1800811228

Johnson, R.L., Wilson, C.G., 2018. A review of vagus nerve stimulation as a therapeutic intervention. J. Inflamm. Res. 11, 203–213. https://doi.org/10.2147/JIR.S163248

Kalia, M., Mesulam, M. -M, 1980. Brain stem projections of sensory and motor components of the vagus complex in the cat: II. Laryngeal, tracheobronchial, pulmonary, cardiac, and gastrointestinal branches. J. Comp. Neurol. 193, 467–508. https://doi.org/10.1002/cne.901930211

Kalia, M., Sullivan, J.M., 1982. Brainstem Projections of Sensory and Motor Components of the Vagus Nerve in the Rat. J. Comp. Neurol. 211, 248–264.

Leung, Y.Y., Li, L., Hui, Y., Kraus, V.B., 2015. Colchicine --- update on mechanisms of action and therapeutic uses. Semin Arthritis Rheum 45, 341–350. https://doi.org/10.1016/j.semarthrit.2015.06.013.Colchicine

Lin, Y.J., Koretsky, A.P., 1997. Manganese ion enhances T1-weighted MRI during brain activation: An approach to direct imaging of brain function. Magn. Reson. Med. 38, 378–388. https://doi.org/10.1002/mrm.1910380305

Martin, J., Johnston, B.M., Gluckman, P.D., 1991. Central projections of the nodose ganglion and the origin of vagal efferents in the lamb. J. Anat. 175, 105–129.

Merritt, J.E., Jacob, R., Hallam, T.J., 1989. Use of Manganese to Discriminate between Calcium Influx and Mobilization from Internal Stores in Stimulated Human Neutrophils *. J. Biol. Chem. 264, 1522–1527.

Narita, K., Kawasaki, F., Kita, H., 1990. Mn and Mg influxes through Ca channels of motor nerve terminals are prevented by verapamil in frogs. Brain Res. 510, 289–295. https://doi.org/10.1016/0006-8993(90)91379-U

Paulon, E., Nastou, D., Jaboli, F., Marin, J., Liebler, E. and Epstein, O., 2017. Proof of concept: short-term non-invasive cervical vagus nerve stimulation in patients with drug-refractory gastroparesis. *Frontline Gastroenterology*, *8*(4), pp.325-330.

Pautler, R.G., 2004. In vivo, trans-synaptic tract-tracing utilizing manganese-enhanced magnetic resonance imaging (MEMRI). NMR Biomed. 17, 595–601. https://doi.org/10.1002/nbm.942

Pautler, R.G., Koretsky, A.P., 2002. Tracing Odor-Induced Activation in the Olfactory Bulbs of Mice Using Manganese-Enhanced Magnetic Resonance Imaging. Neuroimage 16, 441–448. https://doi.org/10.1006/nimg.2002.1075

Pautler, R.G., Mongeau, R., Jacobs, R.E., 2003. In Vivo Trans-Synaptic Tract Tracing From the Murine Striatum and Amygdala Utilizing Manganese Enhanced MRI (MEMRI). Magn. Reson. Med. 50, 33–39. https://doi.org/10.1002/mrm.10498

Pautler, R.G., Silva, A.C., Koretsky, A.P., 1998. In vivo neuronal tract tracing using manganese-enhanced magnetic resonance imaging. Magn. Reson. Med. 40, 740–748. https://doi.org/10.1002/mrm.1910400515

Peña, D.F., Engineer, N.D. and McIntyre, C.K., 2013. Rapid remission of conditioned fear expression with extinction training paired with vagus nerve stimulation. *Biological psychiatry*, *73*(11), pp.1071-1077.

Poole, D.S., Doorenweerd, N., Plomp, J.J., Mahfouz, A., Reinders, M.J.T., van der Weerd, L., 2017. Continuous infusion of manganese improves contrast and reduces side effects in manganese-enhanced magnetic resonance imaging studies. Neuroimage 147, 1–9. https://doi.org/10.1016/j.neuroimage.2016.09.030

Ryu, S., Brown, S.L., Kolozsvary, A., Ewing, J.R. and Ho Kim, J., 2002. Noninvasive detection of radiation-induced optic neuropathy by manganese-enhanced MRI. *Radiation research*, *157*(5),

pp.500-505.

Saleem, K.S., Pauls, J.M., Augath, M., Trinath, T., Prause, B.A., Hashikawa, T. and Logothetis, N.K., 2002. Magnetic resonance imaging of neuronal connections in the macaque monkey. *Neuron*, *34*(5), pp.685-700.

Saper, C.B., Stornetta, R.L., 2015. THE RAT NERVOUS SYSTEM. Chapter 23 630–657.

Silva, A.C., Lee, J.H., Aoki, I., Koretsky, A.P., 2004. Manganese-enhanced magnetic resonance imaging (MEMRI): Methodological and practical considerations. NMR Biomed. 17, 532–543. https://doi.org/10.1002/nbm.945

Sloot, W.N., Gramsbergen, J.B.P., 1994. Axonal transport of manganese and its relevance to selective neurotoxicity in the rat basal ganglia. Brain Res. 657, 124–132. https://doi.org/10.1016/0006-8993(94)90959-8

Smith, S.M., Jenkinson, M., Woolrich, M.W., Beckmann, C.F., Behrens, T.E.J., Johansen-Berg, H., Bannister, P.R., De Luca, M., Drobnjak, I., Flitney, D.E., Niazy, R.K., Saunders, J., Vickers, J., Zhang, Y., De Stefano, N., Brady, J.M., Matthews, P.M., 2004. Advances in functional and structural MR image analysis and implementation as FSL. Neuroimage 23, 208–219. https://doi.org/10.1016/j.neuroimage.2004.07.051

Sjogren, M.J., Hellstrom, P.T., Jonsson, M.A., Runnerstam, M., Silander, H.C.S. and

Ben-Menachem, E., 2002. Cognition-enhancing effect of vagus nerve stimulation in patients with Alzheimer's disease: a pilot study. *Journal of Clinical Psychiatry*, *63*(11), pp.972-980.

Takeda, A., Ishiwatari, S., Okada, S., 1998a. In vivo stimulation-induced release of manganese in rat amygdala. Brain Res. 811, 147–151. https://doi.org/10.1016/S0006-8993(98)00881-6

Takeda, A., Kodama, Y., Ishiwatari, S., Okada, S., 1998b. Manganese transport in the neural circuit of rat CNS. Brain Res. Bull. 45, 149–152. https://doi.org/10.1016/S0361-9230(97)00330-4

Tjälve, H., Henriksson, J., Tallkvist, J., Larsson, B.S. and Lindquist, N.G., 1996. Uptake of manganese and cadmium from the nasal mucosa into the central nervous system via olfactory pathways in rats. *Pharmacology & toxicology*, *79*(6), pp.347-356.

Valdés-hernández, P.A., Sumiyoshi, A., Nonaka, H., Haga, R., Ogawa, T., Iturria-medina, Y., Riera, J.J., Kawashima, R., Roche, A., Medical, S., 2011. An in vivo MRI template set for morphometry , tissue segmentation , and fMRI localization in rats. Front. Neuroinform. 5, 1–19. https://doi.org/10.3389/fninf.2011.00026

Van Der Linden, A., Verhoye, M., Van meir, V., Tindemans, I., Eens, M., Absil, P., Balthazart, J., 2002. In Vivo Manganese-Enhance Magnetic Resonance Imaging Reveals Connections and Functional Properties of the Songbird Vocal Control System. Neuroscience 112, 467–474.

Vousden, D.A., Cox, E., Allemang-Grand, R., Laliberté, C., Qiu, L.R., Lindenmaier, Z., Nieman, B.J., Lerch, J.P., 2018. Continuous manganese delivery via osmotic pumps for manganese-enhanced mouse MRI does not impair spatial learning but leads to skin ulceration. Neuroimage 173, 411–420. https://doi.org/10.1016/j.neuroimage.2018.02.046

Wang, W., Xu, H., Li, Y., Ma, Z., Sun, X., Hu, Y., 2016. Dose response and time course of manganese-enhanced magnetic resonance imaging for visual pathway tracing in vivo. Neural Regen. Res. 11, 1185–1190. https://doi.org/10.4103/1673-5374.187065

Watanabe, T., Michaelis, T. and Frahm, J., 2001. Mapping of retinal projections in the living rat using high-resolution 3D gradient‐echo MRI with Mn2+‐induced contrast. *Magnetic Resonance in Medicine: An Official Journal of the International Society for Magnetic Resonance in Medicine*, *46*(3), pp.424-429.

Figures

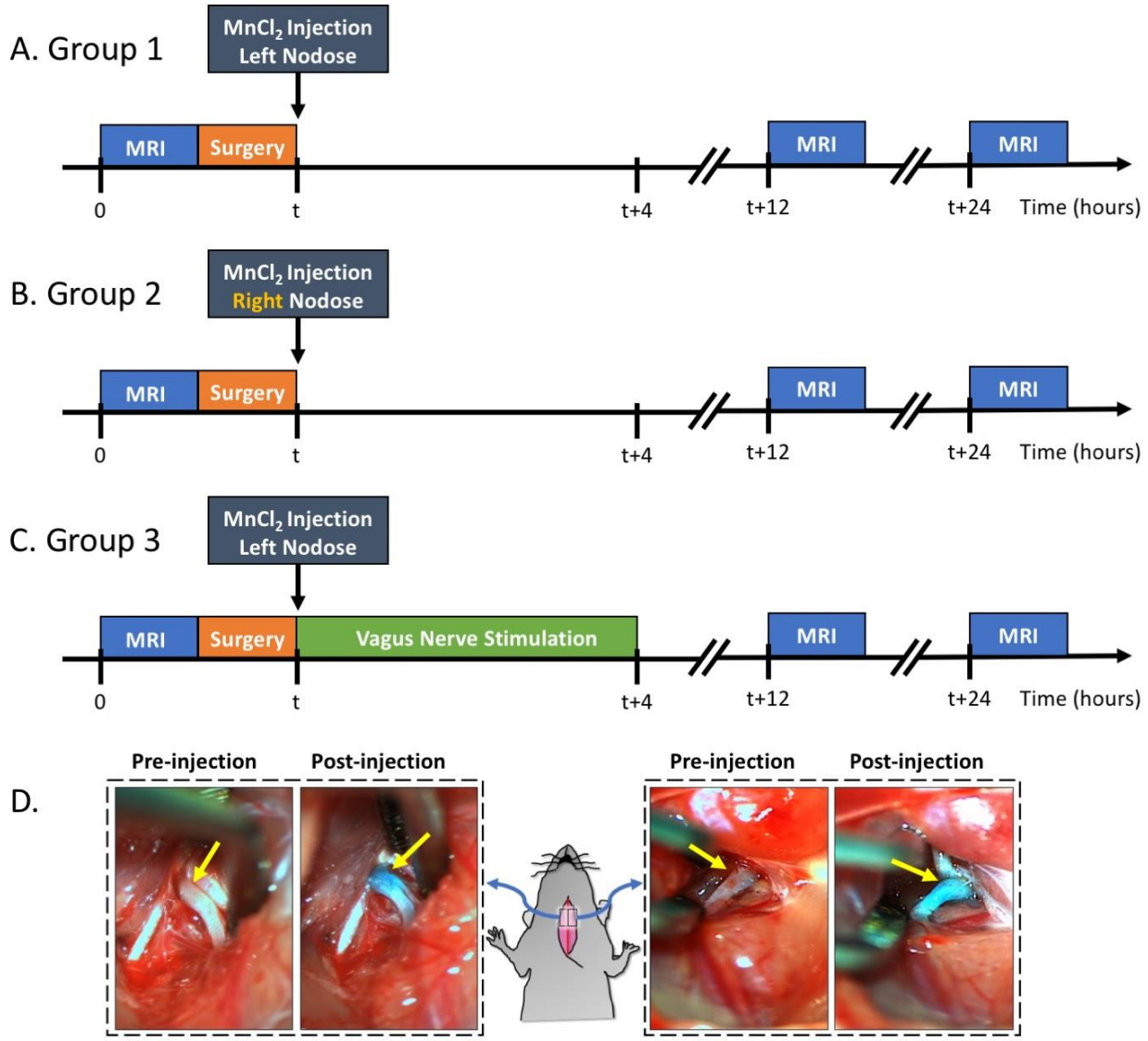

Figure 1. Experiment design and examples of nodose ganglion injection. A, B, and C illustrate the experiment timelines for groups 1, 2, and 3, respectively. For all three groups, the time of nodose ganglion injection is marked as t. The time of VNS and imaging sessions are marked relative to the time of nodose ganglion injection. D presents the right and left nodose ganglion before and after $MnCl_2$ injection. The nodose ganglion occurs as green after injection because of the green dye added to the $MnCl_2$ solution.

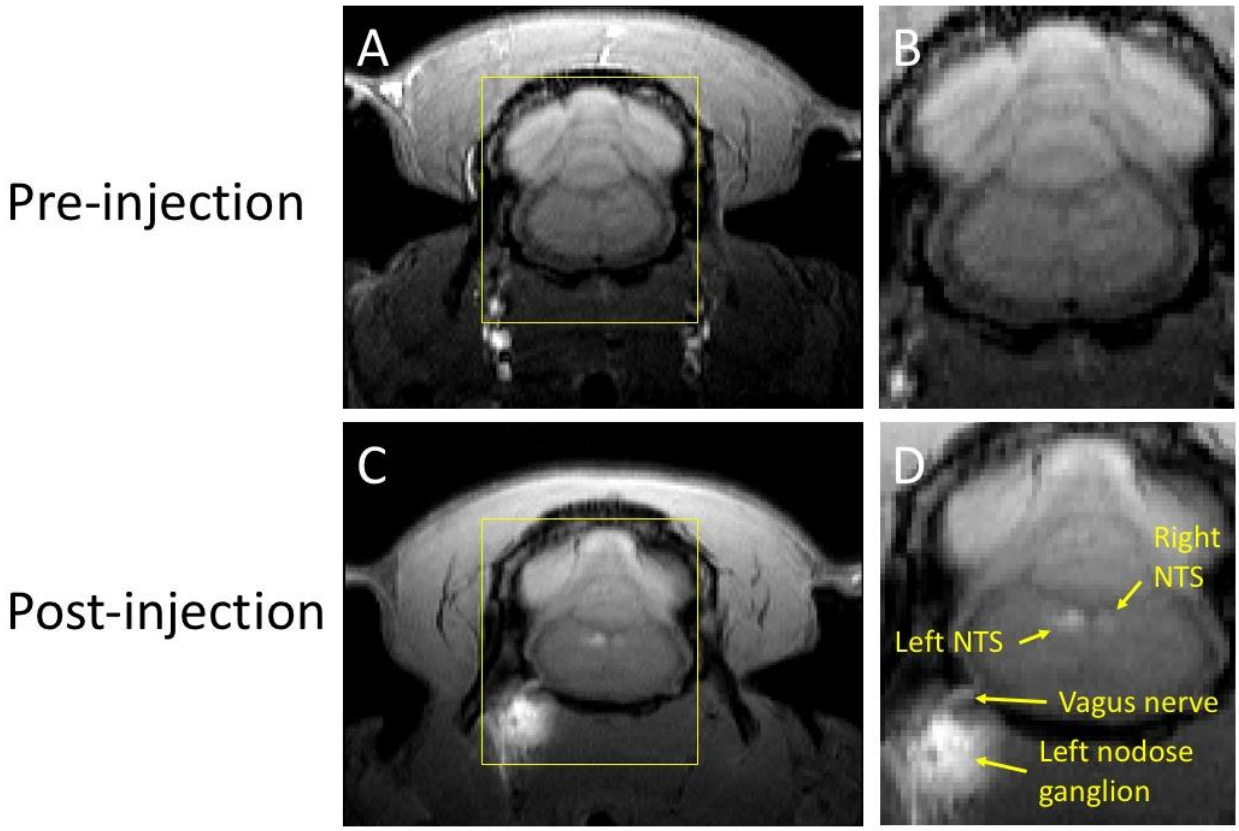

Figure 2. Comparison of T1-weighted images before and after nodose ganglion injection of $MnCl_2$. A & B show T1-weighted images before nodose ganglion injection. B is the zoomed rat brain highlighted in a yellow box from A. C & D show T1-weighted images 24 h after injecting $MnCl_2$ to the left nodose ganglion. D is the zoomed rat brain highlighted in a yellow box from C. The nodose ganglion, vagus nerve, and NTS are marked with yellow arrows in D. Higher signal intensity could be observed in those regions compared to the pre-injection image (B).

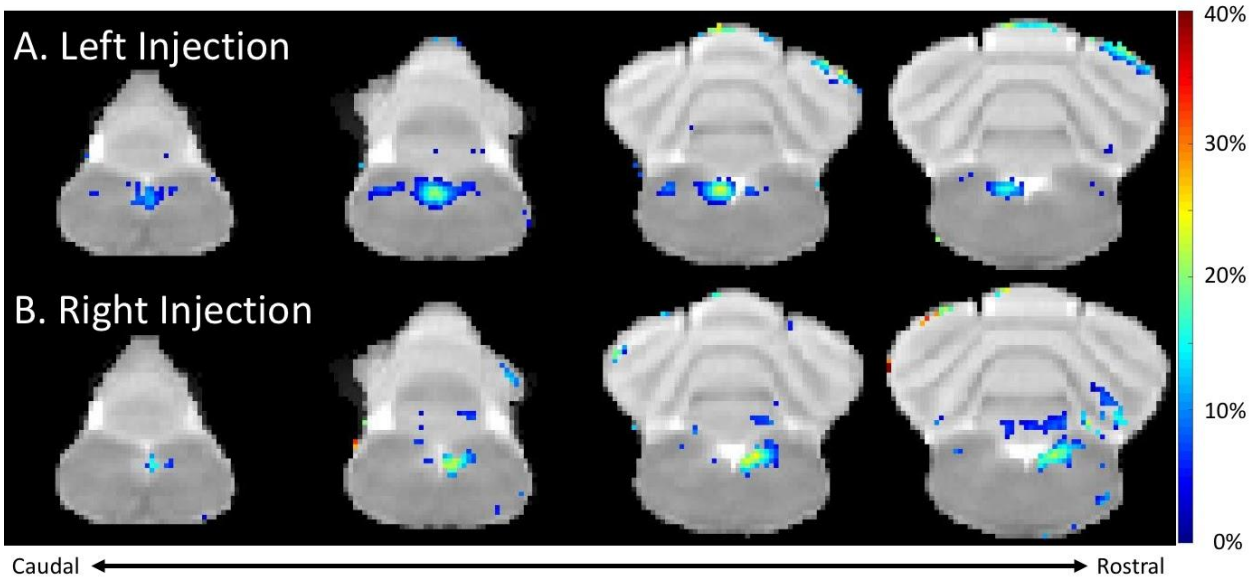

Figure 3. Comparison of T1-weighted intensity increase after left and right nodose ganglion injection. A & B summarize the averaged intensity increase in the rat brain at 12 h after nodose ganglion injection of $MnCl_2$ on the left and right side (group 1 vs. group 2), respectively. Group 1 has the injection on the left nodose ganglion, while group 2 is on the right. These four slices only include the caudal part, mainly covering the brainstem. Statistically significant voxels (right-tailed paired t-test, $p<0.02$) are highlighted and color-coded with their relative intensity increase averaged across all animals within the group.

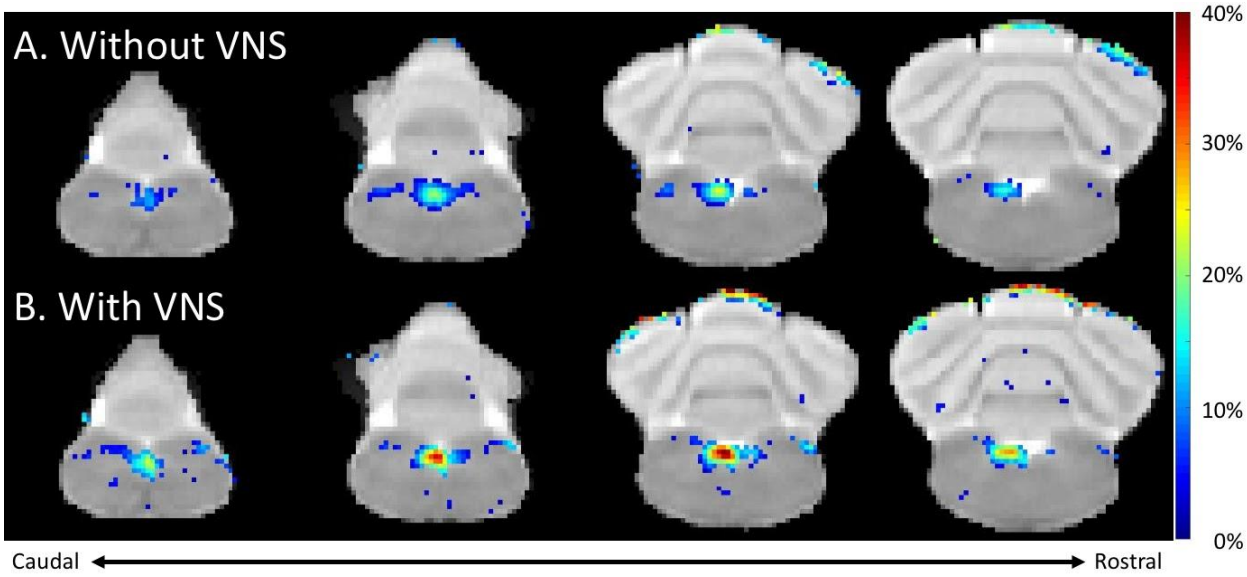

Figure 4. Comparison of T1-weighted intensity increase with and without VNS. A & B summarize the averaged relative intensity increase in the rat brainstem at 12 h post-injection with and without VNS (group 1 vs. group 3), respectively. Group 3 includes VNS lasting for 4 h, while group 1 does not. Both groups have the nodose ganglion injection on the left side. Statistically significant voxels (right-tailed paired t-test, $p<0.02$) are highlighted and color-coded with their relative intensity increase averaged across all animals within the group.

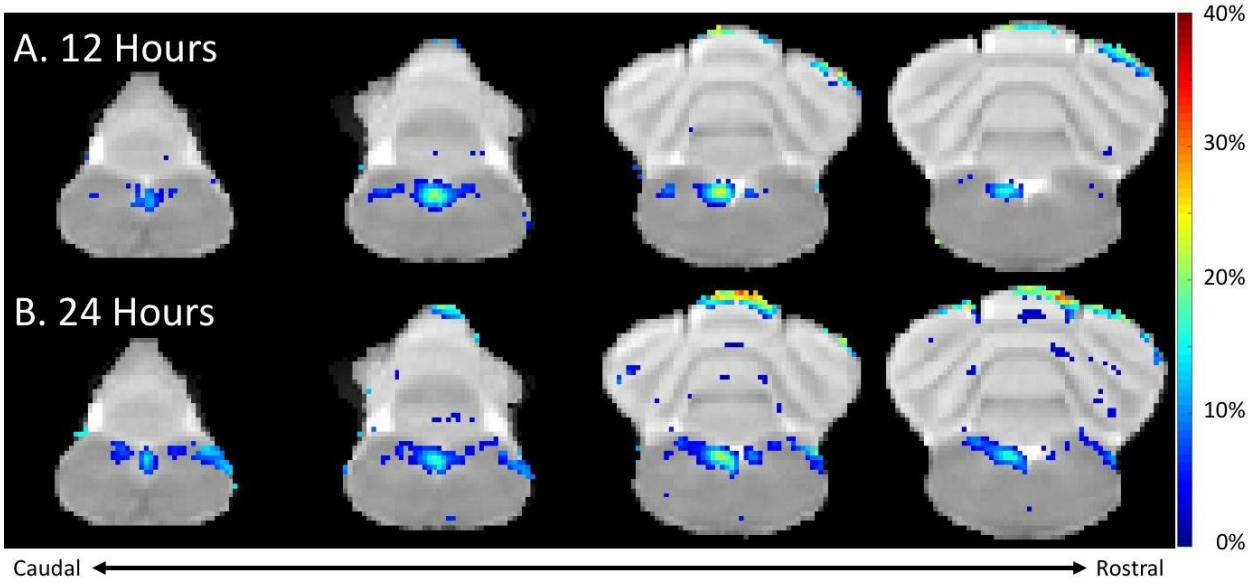

Figure 5. Comparison of T1-weighted intensity increase at 12 h and 24 h post-injection for group 1. A & B show the averaged relative intensity increase in the rat brainstem at 12 h and 24 h post-injection in the left nodose ganglion, respectively. Statistically significant voxels (right-tailed one-sample t-test, $p<0.02$) are highlighted and color-coded with their relative intensity increase averaged across all animals within the group.

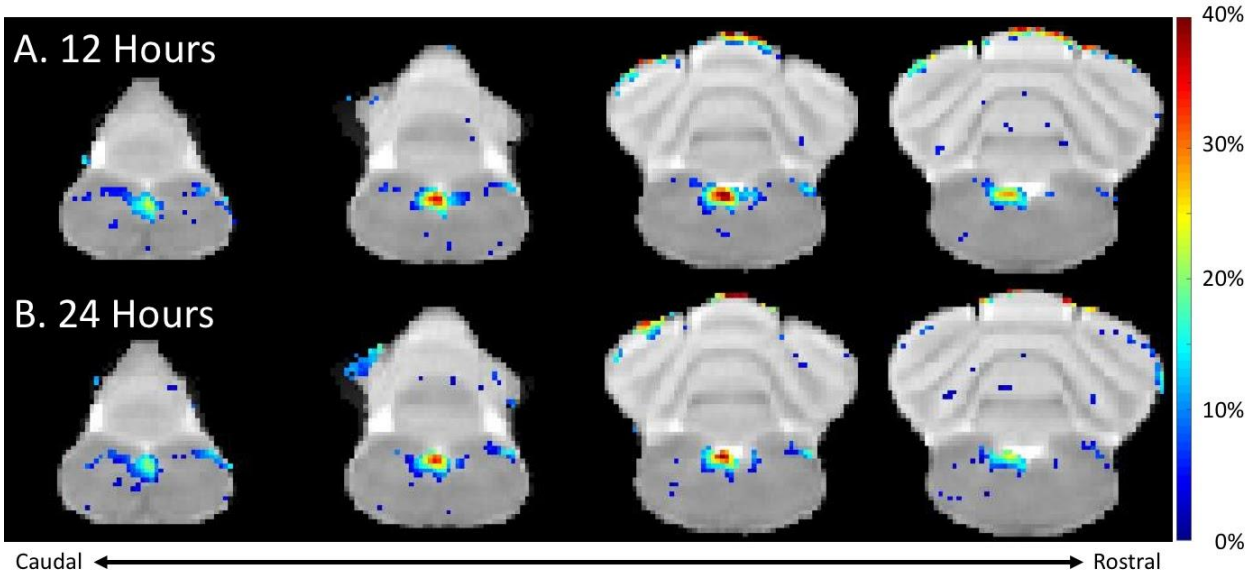

Figure 6. Comparison of T1-weighted intensity increase at 12 h and 24 h post-injection for group 3 (rats received VNS). A & B show the averaged intensity increase in the rat brainstem at 12 h and 24 h post-injection in the left nodose ganglion, respectively. Rats also underwent VNS for 4 h right after the injection. Statistically significant voxels (right-tailed paired t-test, $p<0.02$) are highlighted and color-coded with their relative intensity increase averaged across all animals within the group.

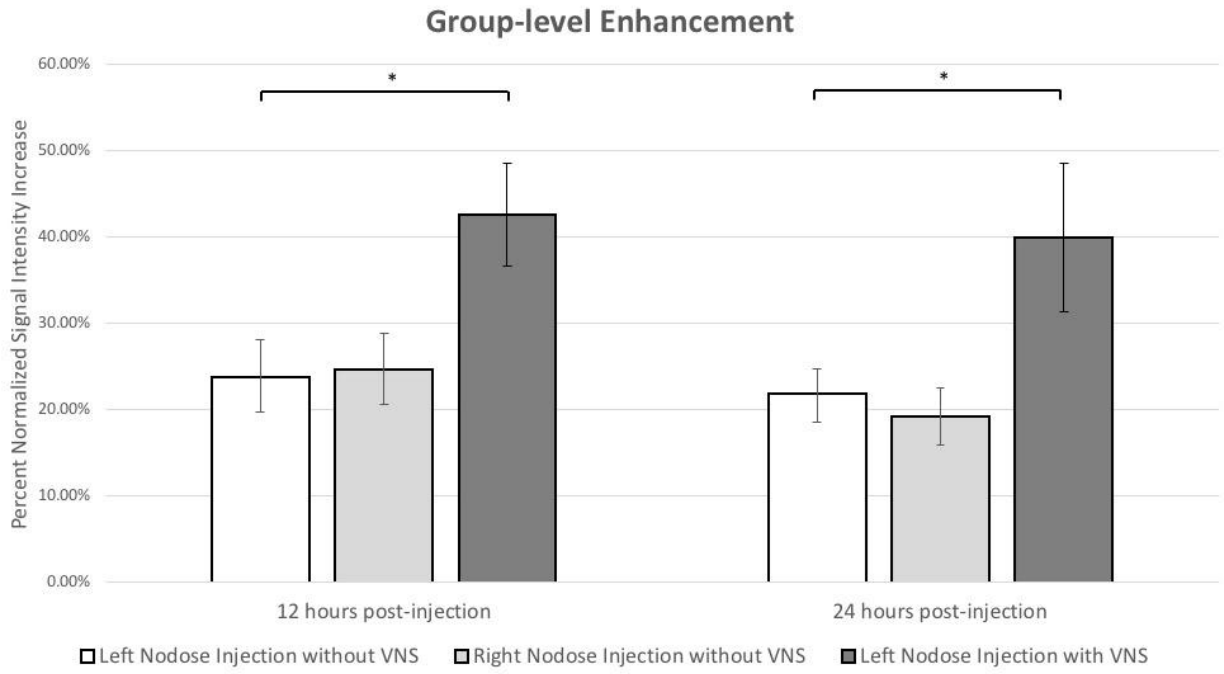

Figure 7. The summary of intensity increase in NTS on the ipsilateral side of nodose ganglion injection. The bar plot shows the mean and standard deviation of maximum intensity increase within NTS. The comparison includes all three groups. The white bar indicates group 1, where rats received left nodose ganglion injection but not VNS. The grey bar indicates group 2, where rats received right nodose ganglion injection but not VNS. The black bar indicates group 3, where rats received left nodose ganglion injection and VNS on the same side. The bar plots contain comparisons at both 12 h and 24 h post-injection. * denotes that the difference is statistically significant on the right-tailed two-sample t-test ($p<0.05$).